Preprints of the 19th World Congress
The International Federation of Automatic Control
Cape Town, South Africa. August 24-29, 2014

Estimating temperature in perfused tissue phantoms subject to ultrasound heating

M. Graça Ruano* Helder S. Duarte**

**FCT, University of Algarve, Faro, and, CISUC-University of Coimbra, Portugal (e-mail: mruano@ualg.pt)*
*** Faculty of Sciences and Technology, University of Algarve, Faro, Portugal (e-mail: a34787@ualg.pt)}*

Abstract: Thermal therapies using induced ultrasound temperature require more research on spatial-temporal temperature propagation over tissues to allow non-invasive and more efficient treatment. This article presents a comparison between the temperature variations induced by therapeutic ultrasound (TU) on phantoms including or not a blood vessel and reports the usage of a square fitting curve to estimate the temperature based on the temporal echo shifts (TES) computed from the RF-lines signals collected by an imaging ultrasound (IU). Three in-vitro experiments were developed based on a gel phantom: a homogeneous phantom and two perfused phantoms, one mimicking right hepatic artery the other common carotid artery. Phantoms were heated with a TU device emitting continuously and temperature was measured by thermocouples placed 50 mm distant from TU transducer face. Experimental results show that a 3 mm blood vessel could reduce temperature in more than 50 % if placed at the TU's axial line when compared with non-perfused phantom. Despite all the dependencies, results also show that temperature estimation can be accomplished when a second order polynomial is applied through TES results. This study confirms that TES relates nonlinearly with temperature and constitutes a reliable noninvasive method of monitoring temperature in perfused tissues.

Keywords: Noninvasive temperature estimation, Therapeutic ultrasound, Temporal echo-shift, Image ultrasound, Fitting.

1. INTRODUCTION

The absence of reliable and non-invasive temperature estimation in a precise temporal-spatial location retrain the application of thermal therapies. Thermal ultrasound is one of the most used treatments in physiotherapy. Ultrasound travels through body tissue and a percentage is captured, resulting in heating generation. The degree of absorption depends on the nature of the tissue, the extent of vascularization and the frequency of the ultrasound beams. In what concerns measurement of the effective temperature induced by the ultrasound in tissues, invasive methods are often employed, regardless the existence of unreachable tissue areas, both because of instrumental and clinical reasons.

Among several possibilities, computation of temporal echo-shifts (Simon C. et al. 1998), frequency-shifts (Amini et al. 2005), backscattered energy (Arthur et al. 2005) and frequency-dependent attenuation (Amini et al. 2005), the temporal echo-shifts modality has proven to be a reliable temperature estimator, overcoming the Magnetic resonance instrumentation's (MRI). MRI is still employed as the gold standard definer of the desirable temperature resolution, this is, establishing a maximum absolute error of 0.5ºC within 1 cm^3 as the target resolution (Arthur et al. 2005). Due to the MRI high costs and difficulty to co-operate with other instruments during a clinical procedure, research has been developed towards the usage of temperature dependent features of the backscattered ultrasound signals to estimate tissue temperature.

Previous research performed by authors' team towards tissue temperature estimation based on TES started with mimicked homogeneous tissue (Teixeira et al. 2006) and developed to heterogeneous tissue phantoms (Teixeira et al. 2007). These studies used TES computed from image ultrasound transducer's data to feed a neural network structure supported by a multi-objective genetic algorithm (Teixeira et al. 2008b). However biological tissues are perfused with vessels, therefore investigating how temperature propagates when blood flow through vessels was a must. Perfused phantoms have been used for testing ultrasound imaging resolution (Guessner et al. 2011), and, by mathematical modulation, to quantify perfusion of liver tissues and metastases (Ghanavati et al. 2011). Recent work made in gel-based phantoms perfused by a hepatic artery (Ruano et al. 2013a) and carotid (Ruano et al. 2013b) artery demonstrate that TES methodology is still sensitive to temperature variations although the vessel presence. In this study, similarly to clinical applications, blood flow was evaluated by Doppler spectrum (Wang et al. 2010 and Lai et al. 2010).

The study hereby described aims to estimate temperature propagation inside perfused tissues, at a spatial-temporal level, aiming at precision but using simpler and less computationally demanding estimators than neural network based ones.

The present paper is divided in four sections. The first one describes the issue of this work and its main goals. Section 2 presents all the instrumental setup and temperature estimation methodology. In section 3, results and discussions about the temperature estimation obtained for perfused and non perfused phantoms are presented. Finally section 4 draws conclusions and themes out for our future research lines.

2. MATERIALS AND METHODS

2.1 Instrumental Setup

Primarily an experimental setup capable of combining TU, IU and Doppler (for perfused phantoms) ultrasound equipments and their connection to the data acquisition and monitoring equipments had to be established. After some trials, the proposed experimental setup configurations for the homogeneous and both the perfused phantoms are the ones represented in Figure 1A) and 1B) respectively. The configuration presented in Figure 1B) is particular for the case of the phantom with right hepatic vessel, as explained below. These experimental setups are able to collect measurements of temperature, blood flow spectrum and radio frequency backscattered A-line traces (RF-lines) without data interference. The rectangular box in the center of Fig. 1A) and 1B) represents the phantom. The phantom should me immersed in a water tank to avoid abrupt temperature changes and better coupling between the transducers and the medium, once water works as ultrasound neutral gel.

Temperature is induced by a therapeutic ultrasound (TU) transducer (Sonopulse Generation 2000, Ibramed) (device 1 and 2 in Fig. 1). The TU has an effective area of 3.5 cm^2, being set to operate in continuous mode at 1MHz and intensities were set to vary from 0.1 to 2 W/cm^2. The temperature data were collected by type k thermocouples (device 4 in Fig. 1), with fixed location through all experiments, connected to a digital multimeter (Keithley, 2700/7700) via a cold junction compensation multiplexer (CJC MUX). The pulse/receiver device, connected to GPIB, allows configuration settings for image ultrasound transducer. The RF-lines used to estimate temperature noninvasively were recorded by a 5 MHz IU's transducer (V310SU, Panametrics-NDT, Element size: 0.6 cm diameter) (device 3 in Fig. 1) operating in pulse-echo mode via a pulse/receiver (Panametrics-NDT, 5800 PR) which sends the analog signals to an oscilloscope (Tektronix, TDS2024). Oscilloscope digitizes the signals at a sampling frequency of 50 MHz with each signal composed of 2500 samples.

There are two main mimicked components for all the experiments. The first one is the mimicked human tissue solution (Sato et al. 2003), hereby simply designated by phantom, and the other one is the mimicked blood flow. Phantom solution is composed of glycerin (11%), water (86.5%) and agar (2.5%), all percentages are expressed relative to weight. Mimicked blood flow (Pais 2006) consists of PVC powder (0.91%), glycerol (10.6%), water (84.77%), detergent (0.90%) and sweetener (3.36%), where all percentages are also expressed relative to weight.

A silicone tube (device 6 in Fig. 1B)) simulate a 3 mm blood vessel used for both perfused phantoms. Peristaltic pump (device 9 in Fig. 1B)) mimic human heartbeat and the blood pressure through silicone tube is controlled by means of syringes (device 8 in Figure 1B)). Since we envisaged testing the temperature propagation in hepatic tissue by including in the phantom an artificial vessel mimicking the right hepatic artery, and since the liver is a terminal organ, only the experiments concerning hepatic vessels required the inclusion of a flow resistance unit, this is, device 10 in Figure 1B). Therefore peristaltic pump, volume of simulated blood in the separator funnel (0.6 litters) (device 5 in Fig. 1) and the pressure applied on the syringes were set to enable spectral center frequencies following the typical curves representing the blood flow Doppler spectra of right hepatic artery and common carotid artery.

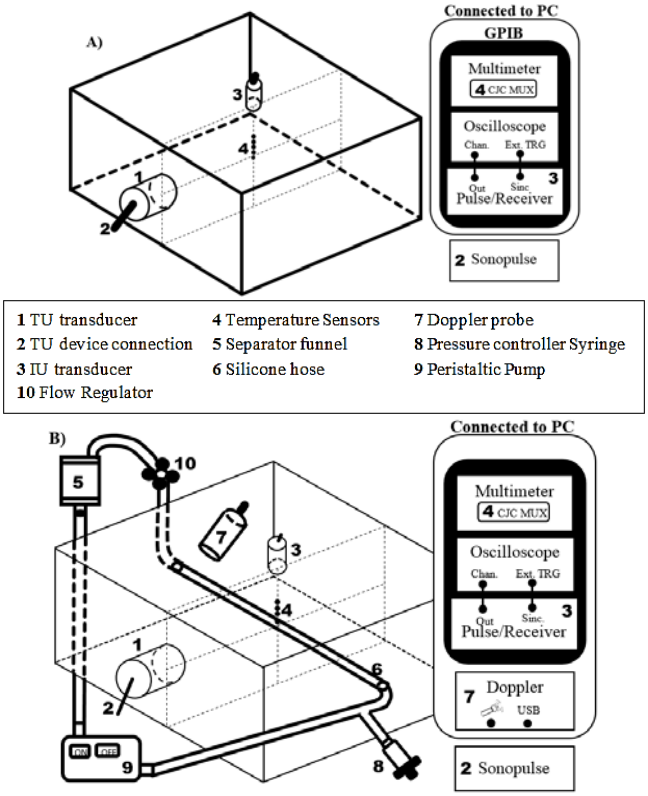

Fig. 1. Experimental configuration developed to estimate temperature for a given TU intensity. A) Homogeneous gel-based phantom. B) Homogeneous gel-based phantom perfused by a hepatic artery.

Doppler frequency signal were acquired by transducer BT8M05 (device 7 in Figure 1B), (positioned at 45º angle with the vessel tube). Doppler signals were recorded as audio files by the personal computer (PC unit in Fig. 1) and processed by a dedicated software package (Pais 2006). The sampling frequency rate used was 22 KHz. All the remaining data were collected by the personal computer via GPIB (GPIB-USB-B, National Instruments).

The signals from multimeter (temperatures) and oscilloscope (RF-lines) were collected every 10 seconds while Doppler signals were recorded during all the experiment, so there

were in total three sets of collected data available and asking for computation. Each experiment took 45 min duration decomposed by three stages: first 5 min for reference measurements, then TU transducer is powered on and ultrasound temperature induced for 20 min, finally TU device is switched off and the phantoms start cooling naturally for another 20 min. Each experiment corresponded to a particular TU intensity applied (0.5, 1.0, 1.5 or 1.8 W/cm^2).

Temperature propagation inside simple homogeneous phantom was evaluated by 5 thermocouples (Fig. 2A)) while perfused phantoms were evaluated by 4 sensors, because sensor S5 was replaced by the blood vessel as Fig. 2B) shows. All sensors were placed in a line 50 mm apart from TU transducer face and thermocouples were 5 mm spaced across the radial line of the TU transducer.

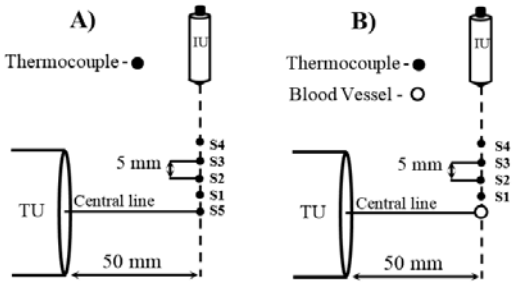

Fig. 2. Thermocouples and blood vessel disposition in relation to IU and TU transducer. A) Homogeneous gel-based phantom. B) Perfused phantoms by carotid artery and hepatic artery.

2.2 Temperature Echo-Shift Methodology

Using the temporal echo-shift as the temperature-dependent feature it was possible to perform temperature evaluation. The strategy applied followed the time-delay estimation presented in (Viola et al. 2005). Considering two segments of the sampled signals $s_1[n]$ and $s_2[n]$ with sizes N and M, respectively, with M<N, signal $s_1[n]$ is called the reference signal, representing in this study the RF-line present in the first backscattered signal. This first echo ($s_1[n]$) is processed to produce an analytical representation, $\hat{s}_1[n]$, using cubic spline coefficients generation. After this, $s_2[n]$ is overlapped N-M times, and a continuous pattern-matching function is computed for each overlap using the sum squared error (SSE) between the two signals ($\varepsilon_i(t)$ for i=1,..,N-M in Fig. 3). Here $s_2[n]$ represent any other RF-line in the backscattered ultrasound signals and ∂ represents the sampling interval. The SSE between two signals is:

$$\varepsilon(t) = \sum_{i=1}^{M} \left(\hat{s}_1(i\partial + t) - s_2[i]\right)^2 = \sum_{i=1}^{M} \left(f_i(t) - s_2[i]\right)^2 \quad (1)$$

The delay is found by taking the derivative of the SSE function with respect to time (Viola et al. 2005). Taking the derivate of $\varepsilon(t)$ with respect to t yields:

$$\begin{aligned} \frac{d\varepsilon(t)}{dt} &= t^5 \sum_{i=1}^{M} 6a_i^2 + t^4 \sum_{i=1}^{M} 10a_i b_i + t^3 \sum_{i=1}^{M} \left(8a_i c_i + 4b_i^2\right) \\ &+ t^2 \sum_{i=1}^{M} \left(6a_i d_i + 6b_i c_i - 6a_i s_2[i]\right) \\ &+ t \sum_{i=1}^{M} \left(4b_i d_i + 6c_i^2 - 4b_i s_2[i]\right) + \sum_{i=1}^{M} \left(2c_i d_i - 2c_i s_2[i]\right) \end{aligned} \quad (2)$$

Setting the result (2) to zero and concentrating all the local delays in a vector (ΔL), the global time-delay estimate can be found. The global estimate is the element from (ΔL) that has a value between 0 and 1, indicating that the true delay is within the tested interval. As the main goal is to estimate temperature for each sensor (at four or five sensors points), a rectangular window was applied to isolate each sensor echo, followed by the correspondent TES computation.

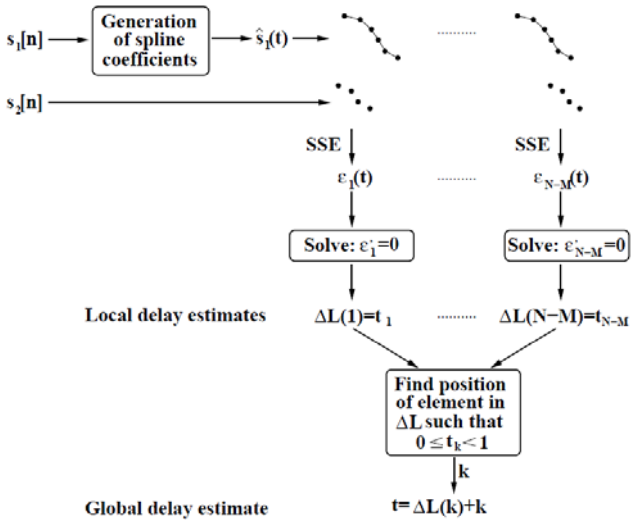

Fig. 3. Schematic representation of the algorithm applied for time-delay estimation where $\varepsilon_i(t)$ is the SSE function associated with the i-th overlap, $\varepsilon_i'(t)$ its correspondent derivate with respect to t and $\Delta L(.)$ the vector containing the local time delay-estimates (t_i). (Teixeira 2008a).

2.3 Temperature Estimation

Once collected the effective temperature and computed the respective temporal echo-shifts for all trials, and, taking into consideration the nonlinear relationship between temperature and TES (as described in next section), square fitting curves have been applied to TES data. Considering a second order equation given by:

$$\bar{y} = a + b\bar{x} + c\bar{x}^2 \quad (3)$$

Where $\bar{y}$ and $\bar{x}$ are data vectors with n values each. Let $y_{\lambda i}$ be the theoretical values for x_i given data. The associated errors are $e_{\lambda i} = y_{\lambda i} - (a + bx_i + cx_i^2)$ which is equivalent to $e_{\lambda i}^2 = (y_{\lambda i} - (a + bx_i + cx_i^2))^2$. Using the least square principle the best curve fit is the one for which the e's are as small as possible i.e. S, the sum of the square of the errors, is a minimum. The value of S is minimum when:

$$\frac{\partial S}{\partial a} = 0 \text{ , } \frac{\partial S}{\partial b} = 0 \text{ , and } \frac{\partial S}{\partial c} = 0 \quad (4)$$

for S given by:

$$S = \sum_{i=1}^{n} (y_{\lambda i} - (a + bx_i + cx_i^2))^2 \quad (5)$$

And a, b, and c values in (3) are given after solving (4).

The temperature estimation for each spatial point and experimental settings is presented in next section.

3. RESULTS

In Fig. 4 some examples of the collected backscattered ultrasound signals during a trial experiment are represented. Although presenting small TU beam interference, the darker vertical traces at Fig. 4 represent the main echoes collected allowing a clear identification about sensors location. As sensor S4 was the sensor closest to the IU transducers' face (see Fig. 2) therefore its echo arrives prior to S3, the second closest sensor to the IU.

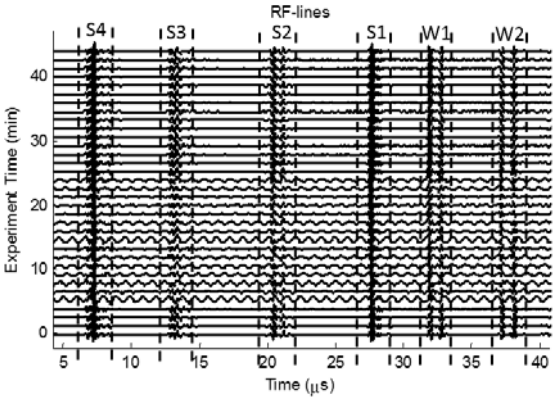

Fig. 4. Imaging Transducer's RF-lines signals collected from the homogenous gel-based phantom perfused by common carotid artery.

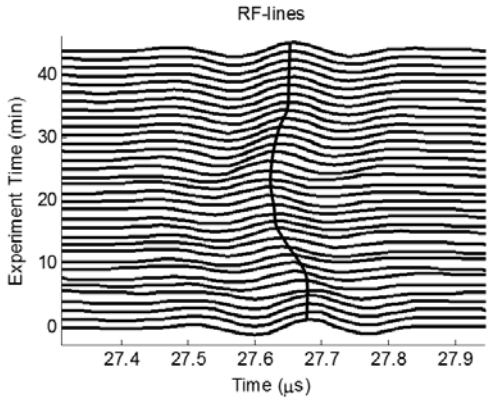

Fig. 5. Detailed view of the echo originated at sensor S1, the vertical curve was introduced just for visual perception of the shifts due temperature variation.

Besides sensors location, Fig. 4 also enables an identification of blood vessels walls W1 and W2 since this figure reports a trial for perfused phantoms; if instead a simple homogeneous phantom was being tested (Fig. 2A) setup)between W1 and W2 would be seen the location of sensor S5.

A detailed view of the echo produced by sensor S1 can be found at Fig. 5. From this figure it is visible the shifts of the echoes during the TU heating stage (5 to 25 min) in comparison to the resting or naturally cooling stage of the experiment.

Recalling that the $s_1[n]$ signal was the first echo, i.e. the RF-line at 0 second experiment time and the other RF-lines were the $s_2[n]$ signals, an example of TES algorithm's results is represented in Fig.6. The left-hand side of this figure plots the effective temperature variation measured by S1 thermocouple and on right the correspondent computed TES signal is shown. As can be seen TES is sensitive to temporal temperature change. Also from the TES plot one can identify the three experimental stages: reference, heating and cooling.

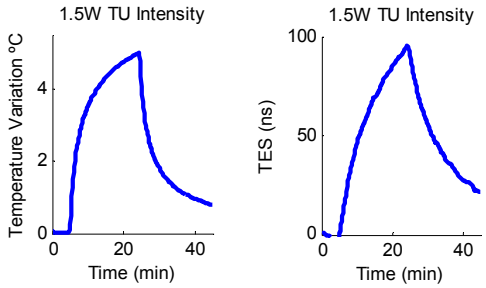

Fig. 6. Comparison between effective temperature variation (left graph) and TES methodology results (right graph) through IU echoes.

When the temperature variation is represented as function of TES (Fig. 7.) the results start at 0, because during the first 5 min of the experiment there were no temperature variations, then the relation describe approximately parabolic curves while temperature increases and decreases, leading to the conclusion that their relationship is nonlinear. Ignoring data related to the first stage of each experiment, this is, before switching on the TU, a square fitting was applied when ultrasound temperature was induced (red line) and another square fitting for the cooling process (black line).

The applied fitting is dependent of spatial location, therapeutic intensity applied and considered phantom. In Fig.7 f(x) and g(x) denote the expressions of square fitting x, the TES values when sensor 1 location is considered and 1.5W TU intensity is applied to a homogeneous phantom. The fitting curve was tuned to allow temperature estimation resolution within the range of the hyperthermia resolution gold standard (MRI resolution), this is 0,5ºC/cm^2. Once f(x) and g(x) equations were established temperature estimates were obtained to each trial performed.

Fig. 8 shows the real temperature variation denoted by blue solid line and heating and cooling estimation process are respectively represented by red and black, following the same color scheme as used in Fig. 7. As can be seen temperature estimation curves are almost overlapped with the measured temperature curves.

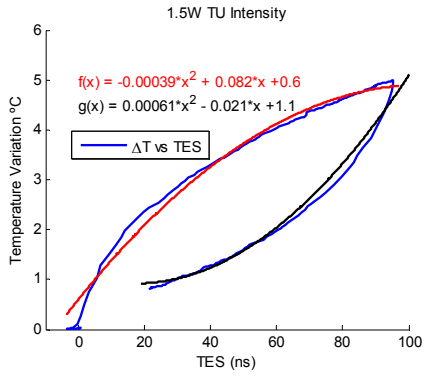

Fig. 7. Temperature variation with respect to correspondent calculated TES (black curve) when 1.5W TU intensity is applied to homogeneous phantom and temperature is measured at sensor S1. Square fitting applied to heating (red curve) and cooling (blue curve) process.

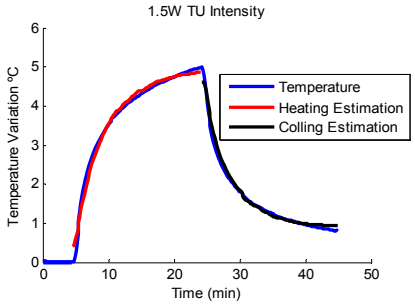

Fig. 8. Example of temperature estimation during heating and cooling procedures.

Fig. 9 enables comparison of the effective temperature variations (measurement based) and the estimated temperatures for different spatial locations inside the simple homogeneous phantom (Fig. 9A), when the phantom is perfused by common carotid artery (Fig. 9B)) and perfused by right hepatic artery (Fig. 9C)).

On these graphs the solid lines represent the temperature variation measured by the thermocouples and the dotted lines express the estimated temperatures using the fitting procedure. Colors differentiate the spatial position, identified by sensors' number: Blue, black, red and green referring respectively to sensors S1, S2, S3 and S4 spatial locations. Sensor S5 has not been considered in Fig. 9 since its location was occupied by the blood vessel on the perfused phantom experiments therefore with no comparative equivalent. As can be seen from Fig. 9A) the highest temperature variation was registered by sensor S1, which is located 50 mm far from TU's face and 5 mm above its axial line. From Table 1 one can see that the temperature estimation at each sensor location is within an absolute error of 0.5 ºC, respecting the MRI gold standard temperature resolution. The highest absolute temperature estimation error was obtained by sensor S1 (0.44ºC) and the smallest was acquired at S4 location (0.04ºC).

Comparing the three graphs of Fig. 9 one can see a general behavioral tracing for heating and for cooling In the case of the phantoms perfused by carotid artery and hepatic artery the range of temperature variations observed at sensor S1 (the spatial location producing higher temperature variations) were shorter than using a simple homogeneous phantom. The experiments with the phantom perfused by hepatic artery achieved the lowest temperature variation range (Fig. 9.C)). Since the perfused phantoms included vessel mimics of the same diameter, the different range of temperature variation is due to the fact that the average blood flow through hepatic vessel is greater than in the common carotid artery (Ruano et al. 2013a).

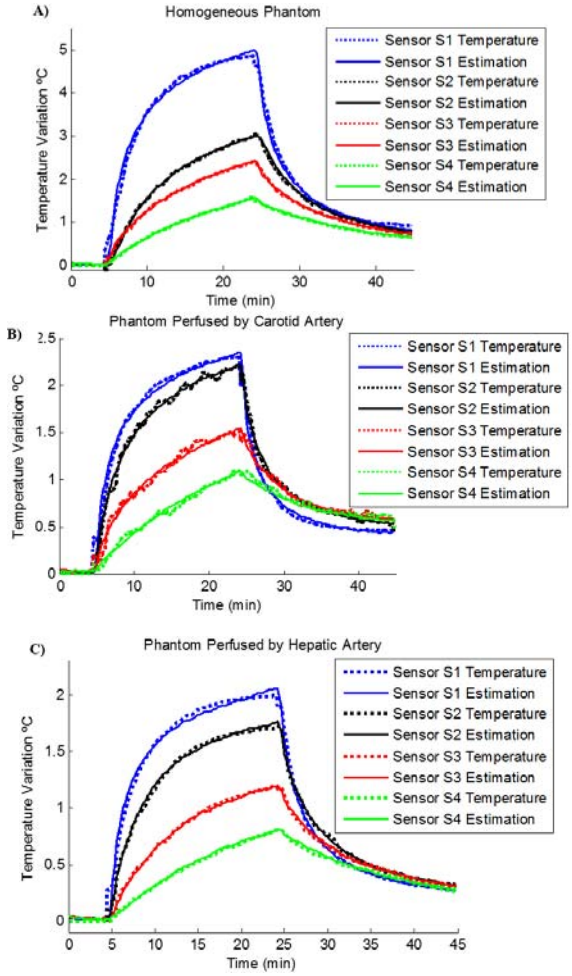

Fig. 9. Effective temperature variations (dotted line) and estimated temperatures (solid line) obtained for: A) simple homogeneous gel-based phantom. B) Homogeneous gel-based phantom perfused by a common carotid artery. C) Homogeneous gel-based phantom perfused by a right hepatic artery, at different spatial points.

In what concerns the errors of temperature estimation, from Table 1 one can see that all experiments produced an absolute error less than 0.5 ºC (see Table 1). It is also identified that the maximum absolute estimation error obtained with the perfused phantoms was 0.36ºC (a value lower than the one obtained with simple phantoms) achieved at sensor S1 location; their minimum absolute error was 0.08ºC at sensor

S4. Also noticeable is the fact that the phantom perfused by the hepatic artery produced the least estimation errors. A common trend of these temperature estimation results is the reduction on estimation errors as the spatial point is deviating from the heating source (TU transducer).

Table 1. Temperature estimation error (ºC).

	S1	S2	S3	S4	
Max	0.38	0.14	0.08	0.06	**A) Simple Homogeneous Phantom**
Min	-0.44	-0.07	-0.10	-0.04	
Max	0.36	0.15	0.16	0.08	**B) Phantom Perfused by Carotid Artery**
Min	-0.36	-0.17	-0.17	-0.08	
Max	0.36	0.15	0.16	0.08	**C) Phantom Perfused by Carotid Artery**
Min	-0.36	-0.17	-0.17	-0.08	

4. CONCLUSIONS

The study hereby described highlights two aspects: a study comparing the temperature variations induced by therapeutic ultrasound on phantoms including or not a blood vessel, and, the usage of a simple square fitting curve to estimate the ultrasound induced temperature based on the temporal echo shifts computed from the RF-lines signals collected by an IT.

The results obtained reveal that mimicked tissue perfused by a hepatic artery and a carotid artery registered a temperature variation decrease of at most 60% and 50% respectively when compared with homogeneous phantom, at a spatial location 50mm far from the TU's face 5mm apart from its central line when a 1.5 W/cm^2 TU power intensity was applied.

The noninvasive temperature estimation procedure using a squared fitting curve, although presenting temperature errors below the gold standard error and being a very simple and computationally efficient estimator revealed that temperature precision depended on the range of temperature variations considered. So, the relation between temperature variation and TES signals is in fact parabolic, both for the heating and cooling process. Research need to be pursued to incorporate spatial location and TU intensity in the temperature estimation model.

REFERENCES

Amini A N, Ebbini E S, and Georgiou T., (2005). Noninvasive estimation of tissue temperature via high-resolution spectral analysis techniques. *IEEE Transactions on Biomedical Engineering*, **52**, 221-228.

Arthur, R. M., Straube, W. L., Trobaugh, J. W., and Moros, E. G., (2005). Noninvasive temperature estimation of hyperthermia temperatures with ultrasound. *Int. J. Hyperthermia*, **21**, 589-600.

Gessner, Ryan C., Kothadia, R., Feingold, S., and Dayton, P., (2011). 3-D Microvessel-mimicking ultrasound phantoms produced with a scanning motion system. *Ultrasound in Medicine & Biology*, **37**, 827-833.

Ghanavati, S., Mousavi, P., Fichtinger. G., and Abolmaesumic, P., (2011). Phantom validation for ultrasound to statistical shape model registration of human pelvis. *Medical Imaging 2011: Image-Guided Procedures and Modelling*, 7964.

Lai, C. Y., Kruse, D. E., Stephens, D. N., Sutcliffe, P. L., and Ferrara, K. W., (2010). Simulation and phantom validation of mild hyperthermia produced by a dual function ultrasound linear array. *IEEE International Ultrasonics Syposium*, 2270-2273.

Pais, P., (2006). User manual: blood flow simulator. *In MsC thesis, UALG*, Unpublished.

Ruano, M. G., and Duarte, H. S., (2013a). Time-spatial ultrasound induced temperature evaluation on perfused phantoms. *The International Conference on Health Informatics*, **42**, 88-91.

Ruano, M. G., Duarte, H. S., Teixeira, C. A., (2013b). Tissue temperature estimation with pulse-echo in blood flow presence. *IEEE 8th International Symposium on Intelligent Signal Processing (WISP)*, 27-31.

Sato, S. Y., W., Pereira, C. A., Vieira, and C.R. S., (2003). Phantom para medição da faixa dinâmica de equipamentos de ultra-som biomédicos. *Revista brasileira de engenharia* biomédica, **19**, 157-166.

Simon, C., VanBaren, P., and Ebbini, E. S. (1998). Two-dimensional temperature estimation using diagnostic ultrasound. *IEEE Ultrasonics, Ferroelectrics, and Frequency Control Society*, **45**, 1088-1099.

Teixeira, C. A., Ruano, M. Graça, Ruano, A. E., Pereira, and W. C. A., (2006). Non-invasive tissue temperature evaluation during application of therapeutic ultrasound: precise time-spatial non-linear modelling. *IFMBE Proceedings*, **14**, 69-72.

Teixeira, C. A., Pereira, W. C. A., Ruano, A. E., and Ruano, M. G., (2007). Narx structures for noninvasive temperature estimation in non-homogeneous media. *IEEE International Symposium on Intelligent Signal Processing*, 169-174.

Teixeira, C. A., (2008a). Soft- computing techniques applied to artificial tissue temperature estimation. *Doctoral thesis, UALG*, Unpublished.

Teixeira, C. A., Ruano, M. G., Ruano, A. E., and Pereira, W. C. A., (2008b). A soft-computing methodology for noninvasive time-spatial temperature estimation. *IEEE Transactions on Biomedical Engineering*, **55**, 169-174.

Viola, F., and Walker, W. F., (2005). A spline-based algorithm for continuous time-delay estimation using sampled data. *IEEE Ultrasonics, Ferroelectrics, and Frequency Control Society*, **52**, 80-93.

Wang, Y., Dan, H. J., Fan, J.H., and Wen, S. B., (2010). Evaluation of the correlation between colour power Doppler flow imaging and vascular endothelial growth factor in breast cancer. *The Jornal of International Medical Research*, **38**, 1077-1083.